Impedance Characterization of Utility-Scale Renewable Energy and Storage Systems

Preprint

Shahil Shah, Przemyslaw Koralwicz, Robb Wallen, and Vahan Gevorgian

National Renewable Energy Laboratory

To be presented at the 2019 Energy Conversion Congress and Exposition (IEEE ECCE)
Baltimore, Maryland
September 29–October 3, 2019

NREL is a national laboratory of the U.S. Department of Energy
Office of Energy Efficiency & Renewable Energy
Operated by the Alliance for Sustainable Energy, LLC

This report is available at no cost from the National Renewable Energy Laboratory (NREL) at www.nrel.gov/publications.

Contract No. DE-AC36-08GO28308

Conference Paper
NREL/CP-5D00-73173
July 2019

Impedance Characterization of Utility-Scale Renewable Energy and Storage Systems

Preprint

Shahil Shah, Przemyslaw Koralwicz, Robb Wallen, and Vahan Gevorgian

National Renewable Energy Laboratory

Suggested Citation
Shah, Shahil, Przemyslaw Koralwicz, Robb Wallen, and Vahan Gevorgian. 2019. *Impedance Characterization of Utility-Scale Renewable Energy and Storage Systems: Preprint*. Golden, CO: National Renewable Energy Laboratory. NREL/CP-5D00-73173. https://www.nrel.gov/docs/fy19osti/73173.pdf.

© 2019 IEEE. Personal use of this material is permitted. Permission from IEEE must be obtained for all other uses, in any current or future media, including reprinting/republishing this material for advertising or promotional purposes, creating new collective works, for resale or redistribution to servers or lists, or reuse of any copyrighted component of this work in other works.

NREL is a national laboratory of the U.S. Department of Energy
Office of Energy Efficiency & Renewable Energy
Operated by the Alliance for Sustainable Energy, LLC

This report is available at no cost from the National Renewable Energy Laboratory (NREL) at www.nrel.gov/publications.

Contract No. DE-AC36-08GO28308

Conference Paper
NREL/CP-5D00-73173
July 2019

National Renewable Energy Laboratory
15013 Denver West Parkway
Golden, CO 80401
303-275-3000 • www.nrel.gov

NOTICE

This work was authored by the National Renewable Energy Laboratory, operated by Alliance for Sustainable Energy, LLC, for the U.S. Department of Energy (DOE) under Contract No. DE-AC36-08GO28308. Funding provided by U.S. Department of Energy Office of Energy Efficiency and Renewable Energy Wind Energy Technologies Office. The views expressed herein do not necessarily represent the views of the DOE or the U.S. Government. The U.S. Government retains and the publisher, by accepting the article for publication, acknowledges that the U.S. Government retains a nonexclusive, paid-up, irrevocable, worldwide license to publish or reproduce the published form of this work, or allow others to do so, for U.S. Government purposes.

This report is available at no cost from the National Renewable Energy Laboratory (NREL) at www.nrel.gov/publications.

U.S. Department of Energy (DOE) reports produced after 1991 and a growing number of pre-1991 documents are available free via www.OSTI.gov.

Cover Photos by Dennis Schroeder: (clockwise, left to right) NREL 51934, NREL 45897, NREL 42160, NREL 45891, NREL 48097, NREL 46526.

NREL prints on paper that contains recycled content.

Impedance Characterization of Utility-Scale Renewable Energy and Storage Systems

Shahil Shah, Przemyslaw Koralewicz, Robb Wallen, and Vahan Gevorgian

National Renewable Energy Laboratory (NREL), Golden, CO 80401, USA
Email: {Shahil.Shah, Przemyslaw.Koralewicz, Robb.Wallen, Vahan.Gevorgian}@nrel.gov

***Abstract*–This paper presents the impedance characterization of utility-scale wind turbines and PV/storage inverters using a multimegawatt grid simulator-based grid integration testbed. The paper describes the testbed components including a 7 MVA grid simulator, 5 MW dynamometer, medium-voltage measurement system, and a real-time control system used for automated impedance characterization of wind turbines and inverters. Different aspects of impedance measurement are discussed, including the selection of the magnitude and type of perturbation, measurement of frequency cross-coupling between sequence impedance responses, and the alignment of the reference frame for sequence impedance measurement. The paper also demonstrates high-fidelity validation of EMT simulation models from turbine manufacturers and characterization of grid-forming inverters using impedance measurements.**

I. Introduction

Cost reductions driven by technological advances continue to increase the penetration levels of inverter-based renewable generation in many power systems around the world. Significant progress is also being made in energy storage technologies to support high penetrations of variable generation from renewable resources. Power electronics is the enabling technology for both renewable energy and storage systems. Unfortunately, the fast dynamics and low overloading capacity of power electronics converters have resulted in many dynamic and transient stability problems, including resonance and control interactions, reduced inertia and frequency response adequacy, deteriorating voltage stability, and tripping of wind and PV power plants during contingency events [1]–[3]. These concerns mandate proper characterization of these new power electronics-based generation and storage technologies before connecting them to the grid.

The impacts of renewable generation and storage on grid stability are usually assessed by grid integration studies using electromagnetic transient (EMT) simulations. The reliability of such studies is highly dependent on the accuracy of the simulated EMT models. Multimegawatt grid simulators are also used to directly test the behavior of wind turbine generators and PV/storage inverters during transient events [4]. One major objective of such testing is to check the compliance of wind turbines and PV/storage inverters with relevant grid interconnection standards. Results from grid simulator testing have also been used by turbine and inverter manufacturers to validate their simulation models. Tests conducted at utility-scale grid-simulator facilities include[†]: i) fault ride-through tests; ii) testing of volt-VAR and frequency-watt characteristics; iii) anti-islanding tests; iv) harmonic emission tests, and v) testing with specific grid impedance (e.g., operation of a Type III wind turbine with a series-compensated transmission line emulated inside the grid simulator). Although these time-domain tests show the actual behavior of the device under test (DUT), it is difficult to obtain much insight into its dynamics. Additionally, these transient tests cannot predict different types of resonance problems the device might experience during different grid conditions, and they also do not support high-fidelity model validation because they do not excite the entire dynamic space of the DUT.

Impedance-based stability analysis is proven effective for the evaluation of control interactions and dynamic stability of converter-based power systems [1]. The impedance response of a DUT is measured by injecting voltage or a current perturbations at different frequencies. Because such perturbations excite the device dynamics over a broad frequency range, they can also be used for high-fidelity validation of EMT models. Until now, however, impedance measurements have been performed only for small- to medium-sized power electronics equipment, particularly for evaluating the stability of shipboard power systems [5]. On the other hand, because of the increasing numbers of control interaction problems in wind and PV power plants, transmission system operators (TSO) have started demanding impedance response data of utility-scale wind turbines and PV inverters from the manufacturers to support thorough evaluation of the impacts on grid stability [1]. Impedance-based specifications are also being developed for wind turbines and PV inverters depending on the grid characteristics at the point of interconnection to reduce the risks of stability problems. Thus, the ability to measure

This work was authored by Alliance for Sustainable Energy, LLC, the manager and operator of the National Renewable Energy Laboratory for the U.S. Department of Energy (DOE) under Contract No. DE-AC36-08GO28308. Funding provided by U.S. Department of Energy Office of Energy Efficiency and Renewable Energy Wind Energy Technologies Office. The views expressed in the article do not necessarily represent the views of the DOE or the U.S. Government. The U.S. Government retains and the publisher, by accepting the article for publication, acknowledges that the U.S. Government retains a nonexclusive, paid-up, irrevocable, worldwide license to publish or reproduce the published form of this work, or allow others to do so, for U.S. Government purposes.

[†]*Proc. 2018 Annual Int. Workshop on Grid Simulator Testing*, Tallahassee, FL, USA provides an excellent overview of utility-scale grid simulator facilities around the world and electrical characterization tests performed at these facilities on wind turbine generators, PV inverters, and energy storage systems [4].

This report is available at no cost from the National Renewable Energy Laboratory (NREL) at www.nrel.gov/publications.

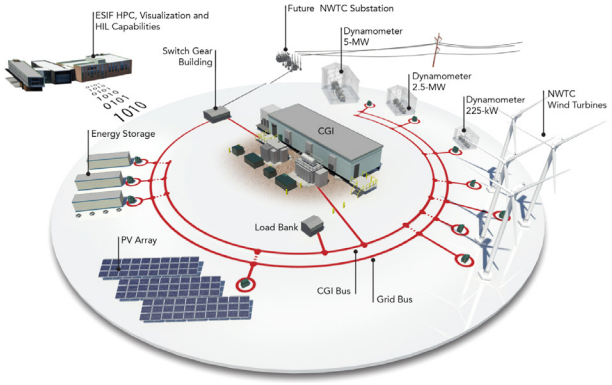

Fig. 1. Infrastructure at NREL centered around a multimegawatt grid simulator for grid-integration research and testing. Illustration by Josh Baurer, NREL.

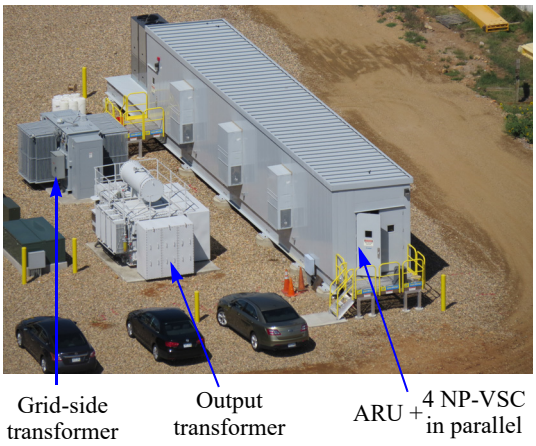

Fig. 2. 13.8 kV, 7 MVA grid simulator called controllable grid interface (CGI) custom designed using ABB's medium voltage ACS6000 drive technology.

impedance responses of utility-scale wind turbines and PV/storage inverters is critical.

This paper demonstrates the impedance measurement of utility-scale wind turbines and PV/storage inverters conducted using a multimegawatt grid simulator-based grid-integration testbed at the National Renewable Energy Laboratory (NREL) in Colorado, USA. The paper describes the testbed components used for the impedance measurement. Different aspects of impedance measurement including the selection of the magnitude and type of injected perturbation, measurement of coupling between positive and negative sequence impedance, and the alignment of the reference frame for sequence impedance measurement are discussed. The paper also presents high-fidelity validation of EMT simulation models and the characterization of grid-forming inverters using impedance measurements.

The rest of the paper is organized as follows: Section II describes the grid-integration testbed at NREL for impedance measurement of utility-scale wind turbines and inverters, Section III presents impedance measurements conducted at NREL and discusses different aspects of impedance characterization, Section IV presents impedance-based validation of EMT models and characterization of grid-forming inverters, and Section V concludes this paper.

II. NREL's Multimegawatt Grid Integration Testbed

Multimegawatt grid simulator is the key technology for testing utility-scale wind turbines and inverters under different grid conditions. First such grid-simulator called controllable grid interface (CGI) was commissioned at NREL in 2013-2014 [6]. CGI is the centerpiece of a grid-integration testbed, which also includes utility-scale wind turbines, PV arrays, battery energy storage systems (BESS), multimegawatt dynamometers for testing wind turbine nacelles, medium-voltage data acquisition system (MVDAS) enabling GPS-synchronized measurements, and digital simulation platforms enabling power-hardware-in-the-loop (PHIL) and controller-hardware-in-the-loop (CHIL) experiments. Fig. 1 shows an illustration of the grid-integration testbed. As shown in the illustration, any combination of devices can be connected to the CGI bus for testing experiments. The following subsections discuss components of the testbed used for impedance characterization.

A. Grid Simulator

The grid simulator (CGI) at NREL is shown in Fig. 2; it is rated for 13.8 kV, 7 MVA continuous power, and 39 MVA short-term rating for 2 seconds. It is custom designed based on ABB's ACS6000 industrial-grade medium voltage drive technology. It features a 9 MVA active rectifier unit (ARU) at the utility-side that regulates the intermediate dc bus voltage. The controllable grid is established by four front-end neutral-point-clamped (NPC) inverters, each with the rated output of 3.3 kV, connected in parallel. A specialized multi-winding output transformer shown in Fig. 2 is used to synthesize 17-level low-distortion voltage waveforms by combining 3-level phase voltages from the inverters. The transformer also steps-up the voltage to 13.8 kV. The CGI is designed to simultaneously meet the following requirements: multimegawatt power rating, sub 1% THD in the voltage waveforms, and extremely fast response time of less than 1 ms. The fast dynamics of CGI enable it to behave like an ideal voltage source that can be used for transient experiments and for injecting perturbations over a broad frequency range for impedance measurements. The control system of the CGI is coupled with an RTDS system, which can provide dynamic voltage references for all three phases and the neutral wire for different grid integration tests; the desired perturbation is configured inside the RTDS system for impedance measurement in different domains [7].

B. Dynamometer for Wind Turbine Testing

Impedance measurements of wind turbine nacelles for specific operation conditions, including active and reactive power output and rotating speed, require a mechanical prime mover that can emulate the behavior of a wind turbine rotor for different wind conditions. A 5 MW dynamometer shown in Fig. 3 is used for this purpose in NREL's grid-integration testbed [8].

This report is available at no cost from the National Renewable Energy Laboratory (NREL) at www.nrel.gov/publications.

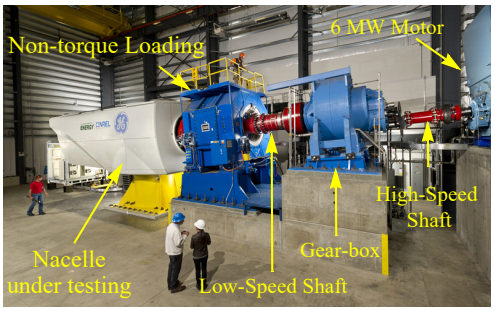

Fig. 3. 5 MW dynamometer for wind turbine nacelle testing.

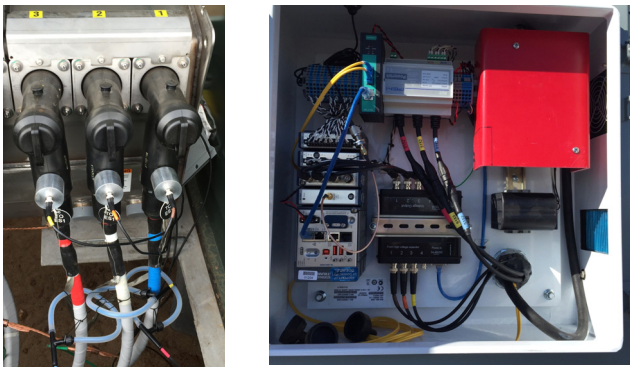

a) b)

Fig. 4. Hardware in each MVDAS sensing node: a) voltage and current sensors; b) data conditioning built around NI 9030 cRIO platform.

C. GPS-Synchronized Medium-Voltage Measurements

The testbed has a medium Voltage Data Acquisition System (MVDAS), which is a distributed network of GPS synchronized measurement nodes sampling three phase voltage and current waveforms at 50 kHz with 24 bit resolution. Raw 50 kHz voltage and current waveform captures can be triggered by programmable thresholds, supervisory control and automation systems, or asynchronously by user interface and stored locally for post event downloading, alignment, and processing. The system is implemented on a National Instruments Compact RIO platform and it utilizes on-board FPGA hardware for synchronization and processing functions. Fig. 4 shows hardware in one of the sensor nodes including capacitive voltage sensors [9], rogowski-coil-based current sensors, and a GPS-synchronized signal conditioning unit built around NI 9030 cRIO platform. MVDAS nodes are located at different points in the testbed shown in Fig. 1 and they allow GPS-synchronized measurement of voltages and currents during injection of perturbations for obtaining an impedance response over a broad frequency range.

D. Impedance Measurement System

To enable impedance measurement of utility-scale power electronics equipment, all components described above are integrated as shown in Fig. 5. The CGI is controlled by an RTDS system using a fast 2 Gbit/s optical fiber interface [10]. The high bandwidth interface and delay compensation techniques implemented in the CGI control system allow injection of perturbations over a wide spectrum of frequencies from 0.1 Hz to 3 kHz. As shown in Fig. 6, a control system is implemented in RTDS for synthesizing voltage references for CGI, consisting of components at the fundamental frequency f_1, perturbation frequency f_p, and mirror frequency $f_m = f_p - 2 \cdot f_1$ [7]. The independent control of components at frequencies f_1, f_p, and f_m is achieved by developing a robust measurement system that can differentiate in real-time the components at all three frequencies, even when these frequencies are as close as 0.5 Hz. The magnitude of the mirror frequency component is regulated to zero to enable accurate measurement of both the direct impedance response and the coupling impedance response [7].

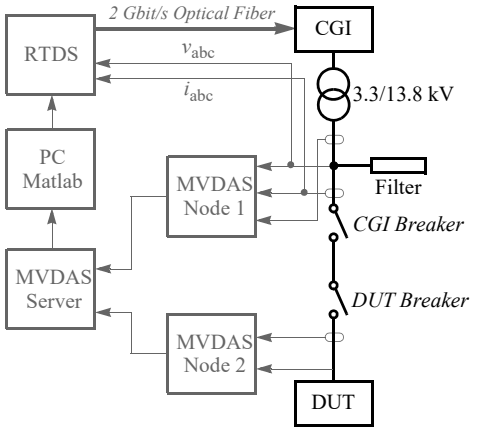

Fig. 5. Impedance measurement system diagram.

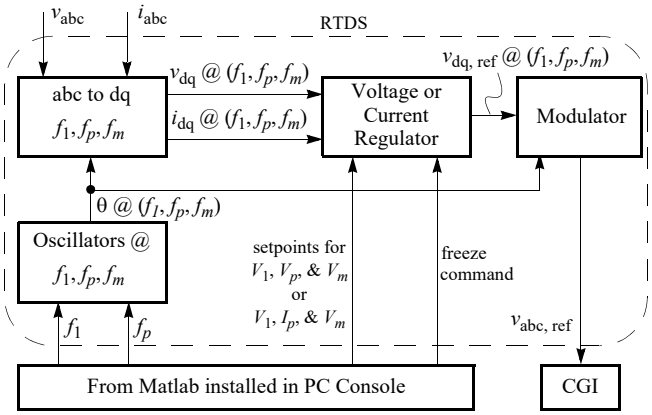

Fig. 6. Control of fundamental, perturbation, and mirror frequency components.

The console PC with Matlab is responsible for automating the impedance measurement process. During initialization, a frequency vector is defined, and CGI and MVDAS are configured. At the beginning of each sequence, a perturbation frequency is selected from the vector and commanded to RTDS to regulate CGI output voltage components at frequencies f_1, f_p, and f_m. After a preset delay time to allow perturbation controllers to reach steady-state, a freeze command is sent to controllers so that their operation does not interfere with data acquisition using MVDAS, which captures a 10s buffer of 50 kHz data on all

This report is available at no cost from the National Renewable Energy Laboratory (NREL) at www.nrel.gov/publications.

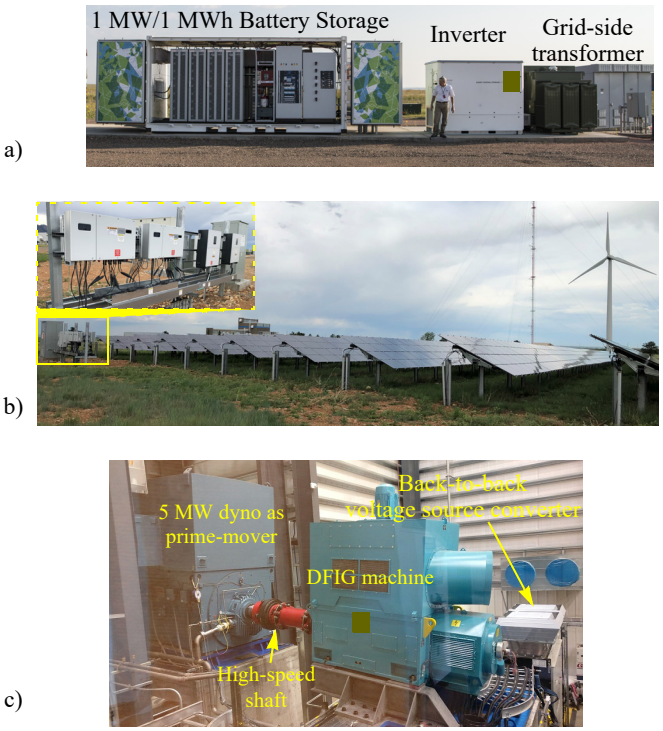

Fig. 7. Test articles for impedance characterization: a) 1 MW/1 MWh battery energy storage system, b) 430 kW PV plant with string inverters, and c) Type-III wind turbine drivetrain of around 4 MW rating.

selected nodes. Once the measurements are recorded for all points in the frequency vector, the system begins post-processing for obtaining an FFT with 0.1 Hz resolution to obtain impedance transfer functions.

III. Impedance Characterization

A. Sequence Impedance Measurement

Fig. 7 shows test articles whose sequence impedance responses are measured using the impedance measurement system described in the previous section. The test articles include a 2 MVA inverter interfacing a 1 MW/1 MWh battery-energy storage system (Fig. 7a), a 430 kW PV plant with six string inverters (Fig. 7b), and a 4 MW Type-III wind turbine drivetrain including a doubly-fed induction generator (DFIG) and back-to-back voltage source converters. The 4 MW DFIG is driven at a constant speed using the 5 MW dynamometer to test its behavior for different wind speeds, particularly for operation at sub-synchronous and super-synchronous rotating speeds.

For positive-sequence impedance measurement of a test article, the CGI injects positive-sequence voltage perturbations superimposed on the nominal fundamental trajectory. Fig. 8 shows voltage perturbation magnitude V_p during three impedance sweeps of the DFIG, demonstrating that the perturbation magnitude is actively regulated during each impedance sweep. Note that V_p in Fig. 8 is represented in terms of the percentage of the nominal peak phase voltage V_1; hence, the magnitude of the

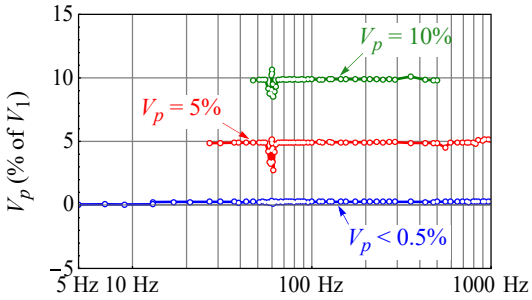

Fig. 8. Magnitude of the injected positive-sequence voltage perturbation V_p injected for three impedance measurement sweeps of a 4 MW DFIG.

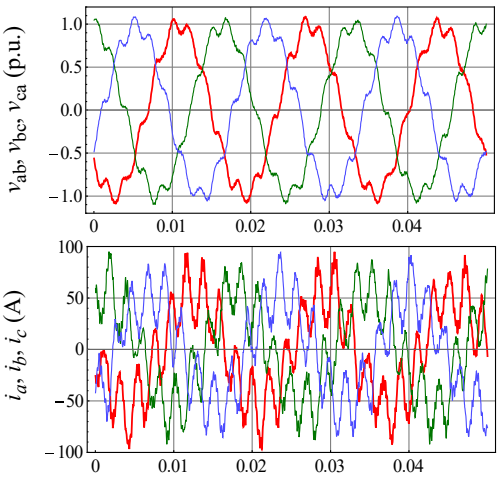

Fig. 9. Line-to-line voltages and output currents of the 4 MW DFIG during injection of 10% positive-sequence voltage perturbation at 477 Hz.

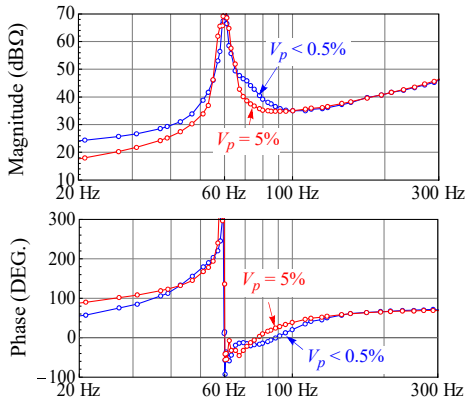

Fig. 10. Positive-sequence impedance response of the 2 MVA BESS inverter shown in Fig. 7a) for different voltage perturbation magnitudes.

injected voltage perturbation in each phase is 1,127 V ($=0.1\cdot\sqrt{2/3}\cdot 13.8\text{x}10^3$) for the 10% perturbation condition. Voltage and current waveforms at the DFIG terminals for a specific perturbation point (f_p = 477 Hz; V_p = 10%) are shown in Fig. 9.

The measured positive-sequence impedance responses of the 2 MVA BESS inverter for different perturbation magnitudes are shown in Fig. 10. The positive-sequence impedance responses of

This report is available at no cost from the National Renewable Energy Laboratory (NREL) at www.nrel.gov/publications.

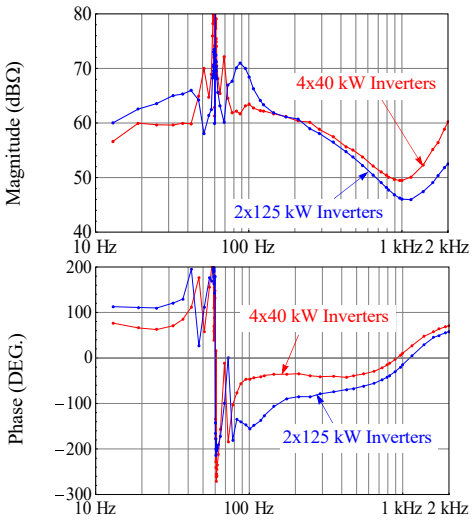

Fig. 11. Positive-sequence impedance response of two sets of string inverters (4x40 kW and 2x125 kW) interfacing a 430 kW PV power plant.

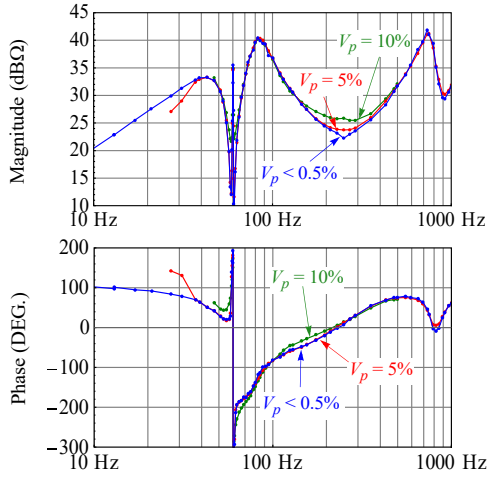

Fig. 12. Positive-sequence impedance response of a 4 MW DFIG-based wind turbine drivetrain for different magnitudes of injected voltage perturbation.

the two groups of string inverters (4x40 kW and 2x125 kW) interfacing the 430 kW PV plant shown in Fig. 7b) are shown in Fig. 11. Fig. 12 shows the positive-sequence impedance responses of the 4 MW DFIG wind turbine drivetrain for different perturbation magnitudes. It can be inferred from the sequence impedance responses in Fig. 10 to 12 that the current control bandwidth of the BESS inverter is around 100 Hz, around 2 kHz for the string inverters in the PV plant, and around 250 Hz for the grid-side converter in the 4 MW DFIG drivetrain. This is inferred from the inductive and capacitive behavior of the impedance responses, respectively, above and below the estimated current control bandwidths. The inductive behavior is because of the phase reactors at the terminals of the BESS inverter, string PV inverters, and the grid-side converter of the DFIG, and the capacitive behavior is because of current control.

As can be seen from Fig. 10 to 12, the CGI-based system can measure impedance responses of utility-scale inverters and wind turbines over a broad frequency range from a fraction of a hertz to couple of kHz. The accuracy of the impedance measurement system is verified by comparing the measured impedance response of a three-phase filter connected at the CGI terminals with the analytical prediction based on the filter parameters.

B. Reference Frame of Sequence Impedance

As shown in [7], because of the time-periodic nature of their dynamics, three-phase power electronics devices usually exhibit frequency cross-coupled response: the injection of a positive-sequence voltage perturbation at frequency f_p produces a positive-sequence response at frequency f_p as well as a negative-sequence response at frequency f_p–$2f_1$; the latter can also be interpreted as positive sequence response at frequency $2f_1$–f_p. Similar cross-coupled response is also present for the injection of negative-sequence perturbations. Stability analysis at frequencies closer to the fundamental frequency must account for these coupling effects [7]. The effects of coupling can be modeled by representing the sequence impedance of a three-phase DUT by a 2x2 transfer matrix [7]:

$$\begin{bmatrix} \hat{I}_p(s+j\omega_1) \\ \hat{I}_n(s-j\omega_1) \end{bmatrix} = \begin{bmatrix} Y_{pp}(s) & Y_{pn}(s) \\ Y_{np}(s) & Y_{nn}(s) \end{bmatrix} \begin{bmatrix} \hat{V}_p(s+j\omega_1) \\ \hat{V}_n(s-j\omega_1) \end{bmatrix} \quad (1)$$

where $s = j2\pi f_p$, and subscripts p and n respectively denote the positive- and negative-sequence components of three-phase voltages and currents at the terminals of the DUT.

The elements of the admittance matrix are related and the terminal behavior of a DUT can be completely described in the sequence-domain using the following two transfer functions [7]:

$$Y_p(s) = \frac{I_p(s)}{V_p(s)} \text{ and } Y_c(s) = \frac{I_n(s-j2\omega_1)}{V_p(s)} \quad (2)$$

where $Y_p(s)$ and $Y_c(s)$ respectively represent the positive-sequence direct admittance and coupling admittance. The coupling admittance $Y_c(s)$ can be measured by extracting the negative-sequence response in the output currents of the DUT at frequency f_p–$2f_1$ when a positive-sequence voltage perturbation is injected at frequency f_p.

The phase response of the coupling admittance $Y_c(s)$ [as well as of $Y_{pn}(s)$ and $Y_{np}(s)$] for each perturbation frequency is dependent on the starting point of the data window used for the FFT analysis. In other words, the phase-response of $Y_c(s)$ is dependent on angle ϕ_{v1} defined in Fig. 13. Since ϕ_{v1} is time-periodic in nature, the phase-response of $Y_c(s)$ is also time-periodic; this is because of the time-periodic nature of the dynamics of power electronic devices interfaced with an ac network. The coupling admittance must be measured for the same value of ϕ_{v1} for each perturbation frequency; this requires synchronization of the FFT window with a specific point on the fundamental trajectory of the voltages at the DUT terminals. However, synchronization of data captures is difficult; instead, a method is presented here to compensate for the non-synchronized

This report is available at no cost from the National Renewable Energy Laboratory (NREL) at www.nrel.gov/publications.

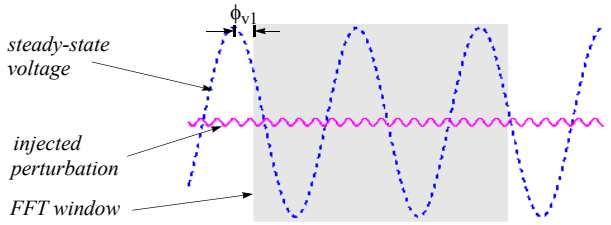

Fig. 13. Reference frame of sequence-domain impedance response.

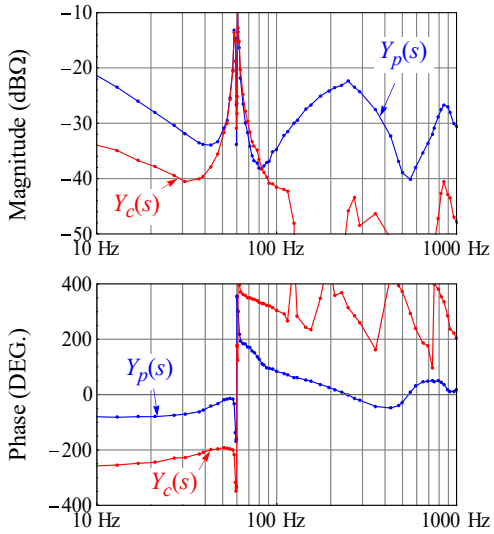

Fig. 14. Frequency cross-coupling between the positive and negative sequence admittance responses of the 4 MW Type III wind turbine drivetrain. Blue lines: response of the positive-sequence direct admittance $Y_p(s)$ and red lines: response of the positive-sequence coupling admittance $Y_c(s)$.

data captures during post-processing of the measurements.

In this paper $\phi_{v1}=0$ is used as the reference frame for the sequence impedance measurement. This is equivalent to aligning the d-axis for dq impedance measurement with the phase-a voltage at the DUT terminals [11]. It can be shown that if

$$\angle Y_c(s)\big|_{\phi_{v1}=0} = \Theta \tag{3}$$

then

$$\angle Y_c(s)\big|_{\phi_{v1}=\alpha} = \Theta - 2\alpha \tag{4}$$

The factor 2α in (4) is the result of the mismatch of $2\omega_1$ in the frequencies of the voltage and current perturbations in the definition of $Y_c(s)$ in (2). Comparing (3) and (4), we get:

$$\angle Y_c(s)\big|_{\phi_{v1}=0} = \angle Y_c(s)\big|_{\phi_{v1}=\alpha} + 2\alpha \tag{5}$$

Eq. (5) can be used to obtain the phase-response of $Y_c(s)$ in the reference frame defined by $\phi_{v1}=0$ by using the phase angle of the fundamental component of the voltages at the DUT terminals obtained by FFT analysis.

Fig. 14 compares measured responses of $Y_p(s)$ and $Y_c(s)$ of the

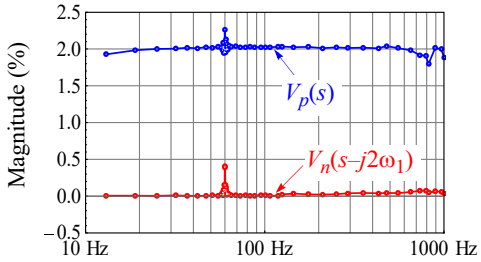

Fig. 15. Active regulation of the magnitudes of the injected positive-sequence voltage perturbation $V_p(s)$ and the mirror negative-sequence voltage perturbation $V_n(s-j2\omega_1)$. In this case $V_p(s)$ is regulated at 2% and $V_n(s-j2\omega_1)$ is regulated at 0% to avoid measurement errors because of the non-negligible CGI impedance.

4 MW DFIG obtained by following the above described alignment process. Clearly, the coupling admittance $Y_c(s)$ is as significant as the direct admittance $Y_p(s)$ around the fundamental frequency. This proves experimentally using a utility-scale wind turbine drivetrain that the evaluation of resonance near the fundamental frequency (<100 Hz) must consider the frequency cross-coupling between the positive- and negative-sequence impedance [7]. Note that $Y_c(s)$ is significantly smaller than $Y_p(s)$ away from the fundamental frequency, implying that the cross-coupling is much smaller, and it can be ignored for the evaluation of stability problems away from the fundamental frequency [7].

Note that the non-negligible internal impedance of CGI may result in a negative-sequence voltage perturbation at frequency f_p-2f_1 because of the coupling current response $I_n(s-j2\omega_1)$ when a positive-sequence voltage perturbation $V_p(s)$ is injected for impedance measurement. This may introduce errors in the impedance measurement. This is avoided by actively regulating the negative-sequence voltage component at the mirror frequency f_m ($=f_p-2f_1$) to zero using the control system shown in Fig. 6. The performance of the control system in eliminating the reflected voltage perturbation at the mirror frequency is shown in Fig. 15; it is evident that the CGI efficiently regulates the injected positive-sequence perturbation magnitude at a specified level (2% in this case) while ensuring that the magnitude of the reflected voltage perturbation at the mirror frequency stays closer to zero.

Note that for the stability analysis of a network around the fundamental frequency, the reference frames of sequence impedance/admittance responses, as defined in (1), for all the components inside the network must be aligned with a global reference frame; this is equivalent to the requirement of reference frame aligned for analysis using dq impedance responses [11].

C. Magnitude and Type of Perturbation

Small-signal impedance measurements are performed by injecting perturbations with magnitudes as small as possible. Small-signal impedance-based stability analysis is effective for the evaluation of control interactions and resonance problems [1]; however, small-signal analysis cannot predict the magnitude of resonance, i.e. the amplitude of resonance-generated distortions, which is important for the protection and control design of

This report is available at no cost from the National Renewable Energy Laboratory (NREL) at www.nrel.gov/publications.

converters and for the estimation of power quality under different operation conditions. As shown in [12], nonlinearities change the impedance response of wind turbines, inverters, HVDC converters, etc., as the perturbation magnitude is increased. The set of impedance responses for different perturbation magnitudes, which is referred to as large-signal impedance in [12], [13], can be used to predict the magnitude of distortions during resonance and control interaction problems. As demonstrated in Figs. 10 and 12, the CGI-based impedance measurement system can actively regulate the magnitude of injected perturbation enabling both small-signal and large-signal impedance measurements.

Impedance sweeps are performed by gradually increasing the injected perturbation magnitude until the DUT starts tripping because of protection. Such a set of impedance responses can not only predict the magnitude of the resonance-generated distortions the device will experience under different grid conditions, but it also characterizes the response of the protection systems to distortions at non-fundamental frequencies. Fig. 8 shows that the range of impedance sweeps of the DFIG starts narrowing as the injected perturbation magnitude is increased. This is because the DFIG starts tripping for the higher perturbation magnitudes, particularly when the perturbation frequency is away from the fundamental frequency. Hence, the large-signal impedance responses also show the range of resonance magnitudes and frequencies that are not sustainable by the test article; the device will trip if any small-signal instability pushes it in the zone where the resonance is not sustainable.

Fig. 8 and 12 show that the 4 MW DFIG does not tolerate high magnitude voltage perturbations in the subsynchronous range. DFIG-based wind turbines are prone to subsynchronous resonance (SSR); it is important to capture the change in their impedance response with the perturbation magnitude in the subsynchronous frequency range to predict the magnitude of the SSR-generated harmonics [14]. The reason for the tripping of the DFIG machine for higher magnitudes of voltage perturbations is the accompanying overcurrent; Fig. 9 exemplifies this behavior, in which the response perturbation in the DFIG output currents is substantially higher than the perturbation injected in the terminal voltages. Hence, the impedance response of a DFIG should be measured such that the magnitude of current perturbation is regulated at a specific level. As shown in Fig. 6, impedance measurement with a constant current perturbation magnitude is achieved by using the regulator for the current perturbation magnitude instead of the voltage perturbation magnitude; the CGI regulates the current perturbation magnitude by modulating the magnitude of the injected voltage perturbation.

IV. Applications

Impedance responses of wind turbines and PV/storage inverters obtained using simulations are being increasingly used for finding root-cause of control interactions and power system oscillations involving by wind and PV power plants [1]. They are also used for control tuning to mitigate resonance issues and develop impedance specifications for wind turbines and PV

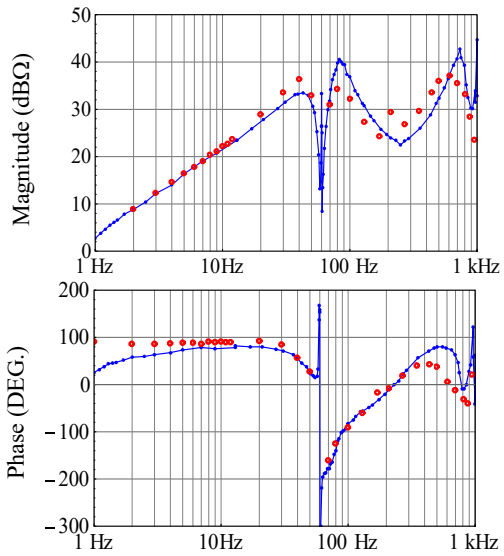

Fig. 16. Positive-sequence impedance response of the 4 MW Type III wind turbine drivetrain obtained by measurements using CGI (blue solid lines) and using simulations of a PSCAD model from the turbine manufacturer (red points).

inverters to reduce the risks of stability problems. The ability to directly measure impedance responses of utility-scale power electronics devices as presented in this paper is important to expand these use cases to support manufacturers for control design. Impedance measurements can also be used by turbine and inverter manufacturers to show compliance with emerging interconnection standards based on impedance response.

Another important application of impedance measurement is it provides a platform for high-fidelity validation of EMT simulation models of multimegawatt wind turbines and inverters. Currently, manufactures validate their EMT models of wind turbines and inverters for power plant design and grid impact studies by comparing the model response with the device response to a transient test conducted at a grid-simulator facility [4]. However, as mentioned before, the time-domain transient tests using a grid-simulator do not excite the entire dynamic space of the device, making the model validation questionable. Impedance measurement excites device dynamics over a broad frequency spectrum, and it can efficiently serve as a model validation tool. Fig. 16 compares the positive-sequence impedance response of the 4 MW DFIG drivetrain shown in Fig. 7c) obtained using a PSCAD model obtained from the manufacture. The impedance response from the PSCAD model matches closely with the measured response, verifying the accuracy of the model. Impedance-validated models can be used to carry out large-scale grid-integration studies, including transient studies such as fault ride-through and dynamic stability studies such as evaluation of control interactions of wind power plants with the transmission network [1]. Manufactuers can also provide impedance-validated simplified models to TSOs for dynamic studies while protecting their proprietary information.

Finally, because impedance measurement thoroughly characterizes the behavior of a device from the grid perspective, it can

This report is available at no cost from the National Renewable Energy Laboratory (NREL) at www.nrel.gov/publications.

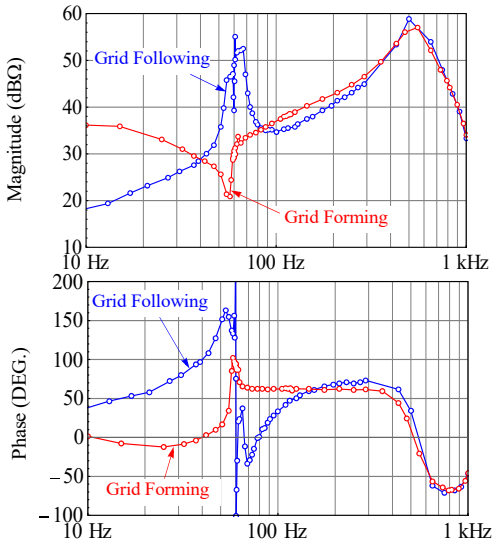

Fig. 17. Positive-sequence impedance response of the 2 MVA BESS inverter shown in Fig. 7a) for its operation in grid-following and grid-forming modes.

be used for characterizing and understanding the impact of new technologies developed for improving grid resilience. For example, recently there has been a lot of interest in grid-forming inverters as a way to substantially increase the penetration of inverter-based generation [15]. Different control methods including droop, virtual oscillator, and virtual synchronous machine-based approaches have been developed for realizing the grid-forming functionality. Impedance characterization can provide an excellent framework for comparing these methods and evaluating their impacts on grid stability. Fig. 17 compares the positive-sequence impedance response of the 2 MVA BESS inverter shown in Fig. 7a) when it is operated in standard grid-following and recently-developed grid-forming control modes. The peaking behavior of the impedance response near the fundamental frequency for the grid-following mode shows that the inverter is being controlled as a current source. On the other hand, the dipping of the impedance response near the fundamental frequency for the grid-following mode shows that the inverter is being controlled as a voltage source. More importantly, the phase-response of the impedance stays relatively closer to zero for the grid-following mode, signifying that the grid-forming mode provides higher damping than the grid-following mode.

V. Conclusion

This paper presented a multimegawatt grid simulator-based testbed for the impedance measurement of utility-scale wind turbines and PV/storage inverters. Different aspects of sequence impedance measurement including the selection of the magnitude and type of the injected perturbation, measurement of the frequency cross-coupling between the positive and negative sequence impedance responses, and the alignment of the reference frame for sequence impedance measurement are discussed. The paper showed that in addition to using impedance measurements for the evaluation and mitigation of dynamic stability problems, they can also be used as a platform for high-fidelity model validation and for characterizing new technologies such as grid-forming inverters. Multimegawatt grid simulator-based impedance measurement systems such as the one presented in this paper will play an important role in future as new interconnection standards emerge for wind and PV power plants based on the impedance response specifications.

References

[1] J. Sun, M. Li, Z. Zhang, T. Xu, J. He, H. Wang, and G. Li, "Renewable energy transmission by HVDC across the continent: system challenges and opportunities," *CSEE J. Power and Energy Syst.*, vol. 3, no. 4, pp. 353-364, Dec. 2017.

[2] "State of reliability," NERC, Atlanta, GA, USA, June 2018.

[3] V. Gevorgian, Y. Zhang, and E. Ela, "Investigating the impacts of wind generation participation in interconnection frequency response," *IEEE Trans. Sustain. Energy*, vol. 6, no. 3, pp. 1004-1012, July 2015.

[4] *Fifth Int. Workshop on Grid Simulator Testing of Wind Turbine Powertrains*, Tallaahasse, FL, USA, Nov. 2018. [Online] Available: https://www.nrel.gov/grid/workshop-grid-simulator-2018-proceedings.html

[5] M. Jaksic, Z, Shen, I. Cvetkovic, D. Boroyevich, R. Burgos, C. DiMarino, and F. Chen, "Medium-voltage impedance measurement unit for assessing the system stability of electric ships," *IEEE Trans. Energy Conv.*, vol. 32, no. 2, pp. 829-841, June 2017.

[6] P. Koralewicz et. al., "Advanced grid simulator for multi-megawatt power converter testing and certification," in *Proc. 2016 IEEE Energy Conv. Cong. Expo. (ECCE)*, 2016, Milwaukee, WI, USA.

[7] S. Shah and L. Parsa, "Impedance modeling of three-phase voltage source converters in DQ, sequence, and phasor domains," *IEEE Trans. Energy Conv.*, vol. 32, no. 3, pp. 1139-1150, April 2017.

[8] S. Lambert, V. Gevorgian, S. Dana, and R. Wallen, "Phase 1 integrated systems test and characterization report for the 5-Megawatt dynamometer and controllable grid interface," NREL, Golden, CO, USA, Tech. Rep. NREL/TP-5000-63073, Mar. 2018.

[9] Jomitek – Powerful Solutions, "The Jomitek v3 voltage sensor," Datasheet, 2012.

[10] P. Koralewicz, V. Gevorgian, and R. Wallen, "Multimegawatt-scale power hardware-in-the-loop interface for testing ancillary grid services by converter coupled generations," in *Proc. 2017 IEEE 18th Workshop on Control and Modeling for Power Electron. (COMPEL)*, Stanford, CA.

[11] A. Rygg, M. Molinas, E. Unamuno, C. Zhang, and X. Cai, "A simple method for shifting local dq impedance models to a global reference frame for stability analysis," available in arXiv, https://arxiv.org/abs/1706.08313, June 2017.

[12] S. Shah and L. Parsa, "Impedance-based prediction of distortions generated by resonance in grid-connected converters," *IEEE Trans. Energy Conv.*, Mar. 2019. doi: 10.1109/TEC.2019.2904674

[13] S. Shah, et. al., "Large-signal impedance-based modeling and mitigation of resonance of converter-grid systems," *IEEE Trans. Sustain. Energy*, vol. 10, no. 3, pp. 1439-1449, July 2019.

[14] S. Shah, V. Gevorgian, and H. Liu, "Impedance-based prediction of SSR-generated harmonics in doubly-fed induction generators," in *Proc. 2019 IEEE Power Energy Soc. Gen. Meet. (PESGM)*, Atlanta, GA.

[15] B. Kroposki, et. al., "Achieving a 100% renewable grid: operating electric power systems with extremely high levels of variable renewable energy," *IEEE Power Energy Mag.*, vol. 15, no. 2, pp. 61-73, Mar.-April 2017.

This report is available at no cost from the National Renewable Energy Laboratory (NREL) at www.nrel.gov/publications.